Large Scale Fabrication of Gold Nano-Structured Substrates Via High Temperature Annealing and Their Direct Use for the LSPR Detection of Atrazine

ARTICLE *in* PLASMONICS · SEPTEMBER 2012

Impact Factor: 2.24 · DOI: 10.1007/s11468-012-9444-3

5 AUTHORS, INCLUDING:

Kun JIA
Université de Technologie de Troyes
64 PUBLICATIONS **296** CITATIONS
SEE PROFILE

Pierre-Michel Adam
Université de Technologie de Troyes
102 PUBLICATIONS **1,431** CITATIONS
SEE PROFILE

Rodica E Ionescu
Université de Technologie de Troyes
60 PUBLICATIONS **655** CITATIONS
SEE PROFILE

Plasmonics
DOI 10.1007/s11468-012-9444-3

Large Scale Fabrication of Gold Nano-Structured Substrates Via High Temperature Annealing and Their Direct Use for the LSPR Detection of Atrazine

Kun Jia · Jean-Louis Bijeon · Pierre-Michel Adam · Rodica Elena Ionescu

Received: 16 April 2012 / Accepted: 26 August 2012

Abstract The present work is reporting on the fabrication of localized surface plasmonic resonant (LSPR) gold nano-structures on glass substrate by using different high annealing temperatures (500 °C, 550 °C, 600 °C) of initially created semi-continue gold films (2 nm and 5 nm) by the electron beam evaporation technique. Interestingly, well-defined gold nano-structures were also obtained from continuous 8 nm evaporated gold film - known as the value above gold percolated thickness - once exposed to high temperatures. The surface morphology and plasmonic spectroscopy of "annealed" nano-structures were controlled by key experimental parameters such as evaporated film thickness and annealing temperature. By using scanning electron microscopy (SEM) characterization of annealed surface it was noticed that the size and inter-particle distance between nano-structures were highly dependent on the evaporated thin film thickness, while the nanoparticle shape evolution was mainly affected by the employed annealing temperature. Due to the well-controlled morphology of gold nano-particles, prominent and stable LSPR spectra were observed with good plasmon resonance tunability from 546 nm to 780 nm that recommend the developed protocol as a robust alternative to fabricate large scale LSPR surface. An example of a LSPR-immunosensor is reported. Thus, the monoclonal anti-atrazine antibodies immobilizion on the "annealed" gold nano-structures, as well as the specific antigen (atrazine) recognition were monitored as variations of the resonance wavelength shifts and optical density changes in the extinction measurements.

K. Jia · J.-L. Bijeon · P.-M. Adam · R. E. Ionescu (✉)
Laboratoire de Nanotechnologie et d'Instrumentation Optique,
Institute Charles Delaunay, Université de Technologie de Troyes,
UMR-STMR CNRS 6279,
12 rue Marie-Curie, BP2060, 10010, Troyes Cedex, France
e-mail: elena_rodica.ionescu@utt.fr

Published online: 14 September 2012

Keywords Gold nano-structures · Localized surface plasmon resonance · Thermal annealing · Optical biosensor · Atrazine

Introduction

Due to the good chemical stability, excellent catalytic activity and promising optical properties, gold nanoparticles (GNPs) have attracted ongoing research interests both in academic and industrial fields [1–3]. During last decades, a myriad of protocols have been developed to realize the controlled synthesis of GNPs in term of size and shape distribution, dispersion stability and surface functionality [4–6]. Basically, these effective methods can be classified either as physical manipulation (top-down) or as chemical transformation (bottom-up) ones [7]. Typical examples of top-down methods include electron beam lithography [8, 9], laser irradiation [10] and ultrasonic fields [11] mediated GNPs synthesis, while the bottom-up protocols mainly focused on chemical reduction of chloroaurate acid into GNPs in the presence of various reducing and stabilized agents such as citrate in classical Turkevich method [12] and thiol ligands in Brust-Schiffrin method [13]. It should be noted that recently, some green chemistry synthetic routines have been developed [14–16], which are especially interested for biological application of GNPs due to the absence of potential toxic chemicals.

Thanks to the unique optical properties of nano-particles, one emerging topic is their use for the localized surface plasmonic resonance (LSPR) experiments, which occurs when the frequency of incident electromagnetic wave is resonant with collective oscillation of free conductive electrons of metal NPs such as gold [17], silver [18], cooper [19] and aluminum [19], etc. As consequences, the strong light scattering, the appearance of intensive surface plasmon absorption and enhancement of localized electromagnetic field have been well observed

[20–22]. These special photonic properties have found applications in the field of plasmon enhanced luminescence [23], optical biosensor [24], diagnostics [25], bioimaging [26] and photothermal therapy [27].

During the last two decades, considerable effects containing both experimental and theoretical work have been dedicated to study localized surface plasmon resonance (LSPR) properties of gold micro/nano-structures [28]. It is well documented that the plasmonic resonant-peak characteristics including shape, maximum extinction wavelength and amplitude are highly dependent on the size, shape and interparticle distance [29], as well as the surrounding effective refraction index of nano-particle. The later characteristic is conventionally considered as the principle of LSPR based biosensor, in which the targeted biomolecules recognition leads to an increase of the localized refraction index and to a red shift of plasmonic peak [30].

An effective optical biosensor, surface plasmon resonance (SPR) biosensor has already been commercialized and widely used in various fields especially in the life science [31]. However, the applications of LSPR based biosensor has increased considerably over recent years, primary due to their cost-effectiveness and desirable flexibility compared to the SPR biosensor [32]. For example, the measurement of LSPR spectra can be realized through a simple transmission mode, where only traditional optical instruments are required [33]. In term of limit of detection, the performance of LSPR biosensor could be comparable and even superior to that of SPR biosensor, as shown for example in a recent report of LSPR biosensor based on enzyme mediated immunodetection of cancer marker PSA [34].

In regard to the tunability of LSPR resonant-peak, considerable efforts have been invested in constructing optimal metal nano-structures, ranging from synthesis of complex GNPs (nanorod [35], nanoholes [36] and nanocages [37]) to deposition of thin gold film on various substrates (glass [38], silicon [39] and ITO [40], etc.). Among these investigations, the evaporation of thin film on appropriate substrate followed by thermal annealing would be more competitive due to the relatively low cost and potential large-scale fabrication ability. For the transmission mode LSPR configuration, glass is the mostly desirable substrate due to its transparent color and inexpensiveness.

There is a major obstacle for the use of regular glass for deposing thin metal film due to the high instability of the noble metal to the bare glass substrate after exposure to aqueous solutions, solvents and buffers, which are used in the biosensor applications [41]. The instability of gold film deposited on glass substrate has been well documented in literatures [42]. Moreover, the morphology of gold thin film deposited on glass surface was reported to be seriously changed due to immersion in solvents [43], which could lead to the non-specific random LSPR resonant-peak changes and thus deteriorating the measurement reproducibility. As an elegant alternative, Israel Rubinstein et al. have recently developed some protocols to stabilize the binding of thin film of gold on glass surface, including a pre-modification step of glass with silane molecules together with a post-depositing step of a very thin layer of silica [44] and one-step partial embedding of GNPs in glass substrate through high temperature annealing [45].

Herein, we have fabricated gold nano-structures exhibiting strong LSPR properties by electron beam evaporation of thin gold film on commercial glass followed by thermal annealing at high temperatures. The morphology and spectroscopy of obtained LSPR structures were systematically studied under various experimental conditions, such as different film thickness, annealing temperature and thermal history. A model of LSPR biosensor was developed for the detection of atrazine herbicide by employing various bio-functionalization steps.

Experiment

Preparation of Gold Micro/Nano-Structures on Glass Substrate

Classical microscope glass slides (Carl Roth GmbH+Co.KG, Germany) were cut around 25×8 mm^2 and subsequently, used as substrates for gold film deposition. Prior to evaporation, all the glass substrates were placed in a plastic sample holder and washed in the mixture of detergent (Decon 90) and deionized water (2:8, v/v ratio) in an ultrasonication water bath (Elmasonic S30H) at 50 °C for 15 min. Further, the resulted samples were rinsed with excess amount of deionized water, drying under a N_2 stream and subjected to another ultrasonication washing in deionized water at 50 °C for 5 min. Finally, the glass substrates were rinsed three times with deionized water, dried in an oven at 100 °C for 10 min, and exposed to the gold vapors.

For the evaporation step, a special metal mold was designed to hold the clean and dried glass substrates. The metal mold was fixed onto a circular evaporation plate with a diameter of 200 mm. The evaporation was conducted in an evaporator (MEB 400, PLASSYS, France) using the electron beam evaporation mode at ambient temperature under a high vacuum (pressure was around 1.0×10^{-5} Torr). The evaporation rate was adjusted around 0.01 nm/s by slowly changing the current intensity. The gold film thickness was monitored by a build-in quartz crystal sensor. In order to obtain homogenous layers of gold on glass surfaces, the plate was slightly rotated during the evaporation process. Three groups of samples (each one has eight replica) with three different nominative gold film thicknesses (2 nm, 5 nm and 8 nm, respectively) were fabricated. After evaporation, the modified glass samples were transferred in a high temperature oven (Nabertherm, Germany) with accessible temperature range from 30 °C to

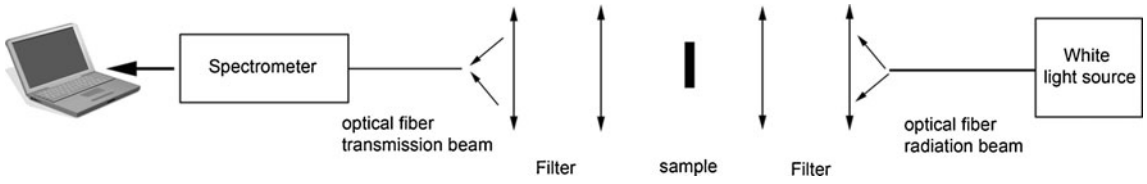

Scheme 1 Transmission LSPR measurement configuration

3000 °C to conduct the annealing procedure in the presence of oxygen. Three different annealing temperatures (in the vicinity of glass transition temperature of glass) of 500 °C, 550 °C and 600 °C were studied in our work. In addition, it was also studied the thermal history influence prior exposure to the desire annealing temperature of as-evaporated gold samples. Experimentally, all the samples of 2 nm film thicknesses were annealed at the same temperature of 550 °C for 8 hrs, but subject to different initial thermal history (e.g. the increasing rate used to get 550 °C from room temperature was 5, 10, 15 and 20 °C/min, respectively).

Biofunctionalization of Gold Nano-Structures

The samples with initially evaporated 2 nm and 5 nm nominated gold thicknesses, annealed at 550 °C for 8 hrs, were used as transducers in the construction of sensitive LSPR-atrazine immunosensors.

The annealed samples were firstly stabilized by washing with ethanol in an ultrasonication bath at room temperature for 20 min and dried under a N_2 stream. Then, the LSPR spectra were recorded as plasmonic references. Further, 100 μL of 0.1 mg/mL monoclonal anti-atrazine antibodies solution diluted in phosphate buffer saline (PBS) was dispersed on the gold nano-structured surfaces to allow incubation at 4 °C for 12 hrs. The resulted antibodies-functionalized surfaces were washed with PBS buffer (pH=7.4) to remove the excess of antibodies. Next, the samples were dried in N_2 stream and their LSPR spectra recorded. Finally, two atrazine antigen dilutions (0.01 and 0.1 mg/mL in PBS) were incubated successively with the antibodies modified-structures for 3 hrs at 4 °C to complete the antibody-antigen interactions. After sample rinsing with PBS buffer and distilled water, the LSPR spectra due to the recognition of the two antigen concentrations by atrazine-antibodies were further recorded and compared.

Gold Nano-Structures Morphology Characterization and their LSPR Investigations

The morphology of freshly-evaporated gold thin films and their corresponding resulted annealed samples were imaged with scanning electron microscopy (SEM, Hitachi S3500N) using an accelerate voltage of 15 kV and a working distance of 5 mm. Photos of gold modified glass samples were captured by a digital camera (Olympus FE-5040). For the LSPR measurements, the experimental configuration was constructed based on transmission UV–vis-NIR spectroscopy as shown in Scheme 1, and contains a white light source (DH-2000-BAC, Ocean Optics), two optic fibers (diameter of 600 μm for radiation beam and 150 μm for transmission beam), and a portable phtotospectrometer (QE65000,Ocean Optics) with a wavelength ranging from 200 nm to 1100 nm, a wavelength sensitivity of 1 nm and a data integration time of 100 ms. The nano-structured glass sample was placed in a homemade sample holder to ensure that the same areas were exposed to the light beam in each LSPR-measurement, and therefore, guarantees the results reproducibility.

Results and Discussion

It is well recognized that the LSPR properties of gold nanostructures are highly influenced by the particle size, shape and interparticle spacing [44, 45]. In the evaporation-annealing protocol, the substrate morphology can be modulated by controlling different experimental conditions such as nominative film thickness, evaporation rate, pressure, annealing atmosphere, temperature and time. In our experiments, two parameters such as nominative thickness of evaporated gold film and annealing temperature, were found to play an important role on the LSPR properties and particles morphology evolutions. Thus, optical spectroscopy and SEM morphology studies were conducted for three different gold film thicknesses (2 nm, 5 nm and 8 nm, respectively) at three different annealing temperatures (500 °C, 550 °C and 600 °C).

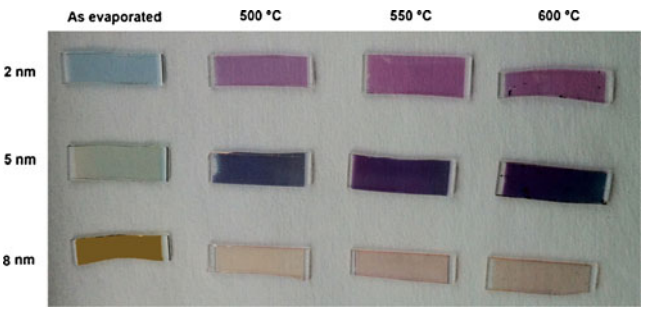

Fig. 1 Photos of glass substrates modified with gold films of three nominative thicknesses (2 nm, 5 nm and 8 nm) before and after annealing at high temperatures (500 °C, 550 °C and 600 °C) for 8 hrs

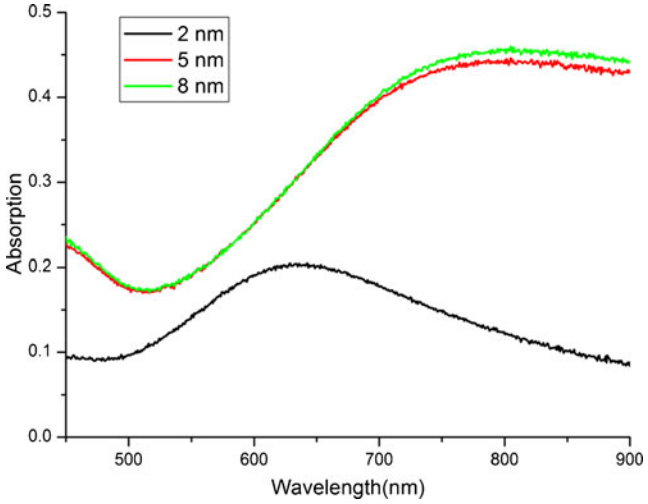

Fig. 2 LSPR spectra of as-evaporated gold sample with different nominative film thicknesses

Influence of the Nominative Gold Evaporated Thicknesses Through the Morphology and LSPR-Spectroscopy of Annealed Gold Nano-Structures

As stated previously in the experimental part, three different nominative thicknesses (2 nm, 5 nm and 8 nm, respectively) of gold films were evaporated. The prepared gold films exhibit different colors changing from light blue for 2 nm to light green for 5 nm and to golden color for 8 nm thicknesses. These colors are changing significantly after the gold samples were annealed at different temperatures for 8 hrs. Experimentally, the high temperature annealing leads to a violet color for the thinnest gold evaporated layer (2 nm), while for the intermediate thickness (5 nm) and thickest deposited film (8 nm) the color emerge from dark blue to orange pink, respectively. Therefore, the higher annealing temperature was used, the darker colors were observed (Fig. 1).

The evaporated film thickness was already reported to play a decisive role in the determination of LSPR properties of gold nano-structures [46]. The LSPR spectra for gold-evaporated sample with three different nominative film thicknesses (2 nm, 5 nm and 8 nm, respectively) were showed in Fig. 2, where a wide extinction peak located at 642 nm with optical density (OD) of 0.2 was observed for the thinnest film of 2 nm. For the other two gold films, the extinction peaks shared almost the same features, that exhibited a minimum OD of 0.17 around 520 nm followed by a large plateau in NIR wavelength range, combined with a slight increase of OD value for 8 nm sample. The wide extinction peak for 2 nm gold sample was attributed to the formation of discrete nano-structures in the very thin evaporated film, while the features of 5 nm and 8 nm sample were considered as typical plasmonic samples of (semi-) continuous film [47].

Although the glass substrates modified with very thin gold films (2 nm) exhibits after annealing process an obvious plasmonic resonant peak according to results in Fig. 2, the gold nano-structures were not very stable because of the weak affinity between gold and glass. To prepare well defined GNPs with stable optical characteristics, a high annealing temperature (close to the glass transition temperature) was conducted in the presence of oxygen. As shown in Fig.3a, the LSPR spectra

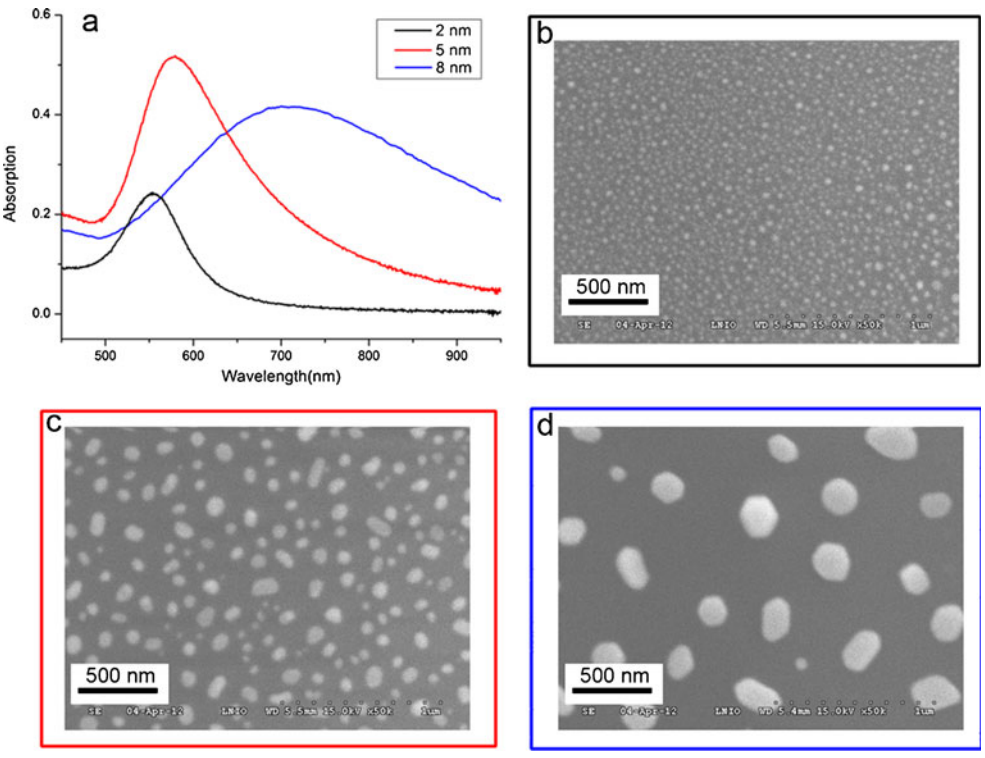

Fig. 3 LSPR spectra of (a) annealed sample with different initial nominative thickness and their corresponding SEM images for 2 nm (b), 5 nm (c) and 8 nm (d). The annealing was conducted in the presence of oxygen at 550 °C for 8 hrs. The SEM images (b, c, d) are in the same scale bar of 500 nm

of the three types of samples with different gold thicknesses changed significantly after annealing at 550 °C for 8 hrs. Interestingly, these annealed samples have well-defined plasmonic peaks. Moreover, by increasing the gold thicknesses, it was noticed that the maximum resonant wavelength was recorded at 553 nm for 2 nm, at 579 nm for 5 nm and at 712 nm for 8 nm sample. Also, it can be remarked that LSPR-peaks became wider with the increasing of gold-evaporated film thickness. There's a maximum plasmonic intensity which was measured for a thickness of 5 nm. This thickness corresponds to nano-particles sizes (see Fig. 3c) which give an optimal extinction coefficient where radiation losses are not too important.

Annealed gold nano-structures were also characterized by SEM microscopy to better understand their morphologies at various temperatures. Fig. 3a shows LSPR spectra while the SEM images of three gold annealed samples with thicknesses of 2 nm, 5 nm and 8 nm at 550 °C for 8 hrs are presented in Fig. 3b, c, and d, respectively. It was noticed that the size of gold nano-particles increased from 30 nm (Fig.3b) to about 400 nm for thickest sample (Fig.3d). Moreover, the interparticle distance also increased as the raising of initial nominative film thickness, e.g. the sample with thicker evaporated film always has less particle density after exposure at high annealing temperature.

It's well known that the maximum LSPR-extinction peak is red-shifted as the nano-particle's sizes increasing [48], which is consistent with our obtained results shown in Fig. 3. Moreover, the shapes of the extinction peaks and their OD values were assumed to be determined by the interplay among particle size, shape and interparticle distance.

Influence of Annealing Temperature Through the Morphology and Plasmonic Spectroscopy of Gold Nano-Structures

Besides the evaporation of various gold thicknesses onto glass substrates, the other investigated parameter important for the construction of sensitive LSPR-measurements was the annealing temperature. Recently, it has been reported that by metal annealing at a temperature close to the transition temperature of the glass substrate would improve the stability of gold created nano-structures [45, 49]. Therefore, we herein conducted systematic studies about the influence of three evaporated gold thicknesses that were annealed at different annealing temperatures through the LSPR measurements. The results are shown in Fig. 4.

Samples with smaller initial film thickness of 2 nm and 5 nm, shared plasmonic peaks with similar evolution as following: at higher annealing temperature, the plasmonic peak was sharper, blue shifted in its resonant wavelength with larger OD value. Specifically, as the annealing temperature increased from 500 °C to 600 °C, the extinction peak was slightly blue shifted from 554 nm to 546 nm with a concomitant amplitude increases of 0.07 OD for thinner gold film (2 nm). In the case of the sample with 5 nm thicknesses (Fig.4b), although the LSPR peaks become wider than that sample with 2 nm (Fig.4a), its amplitude increased (0.06 OD)

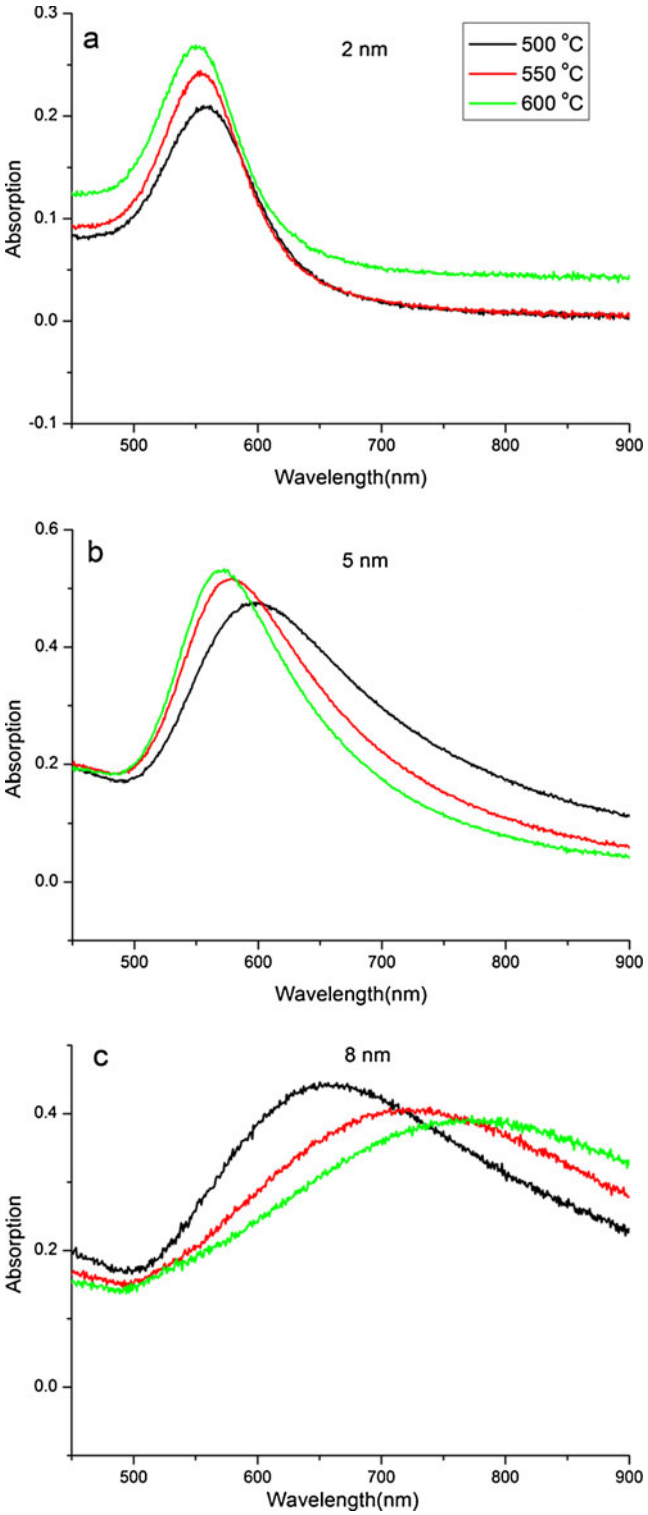

Fig. 4 The LSPR spectra for gold sample annealed samples at three different temperature (500 °C, 550 °C and 600 °C) with nominative film thickness of 2 nm (a), 5 nm (b) and 8 nm (c), respectively

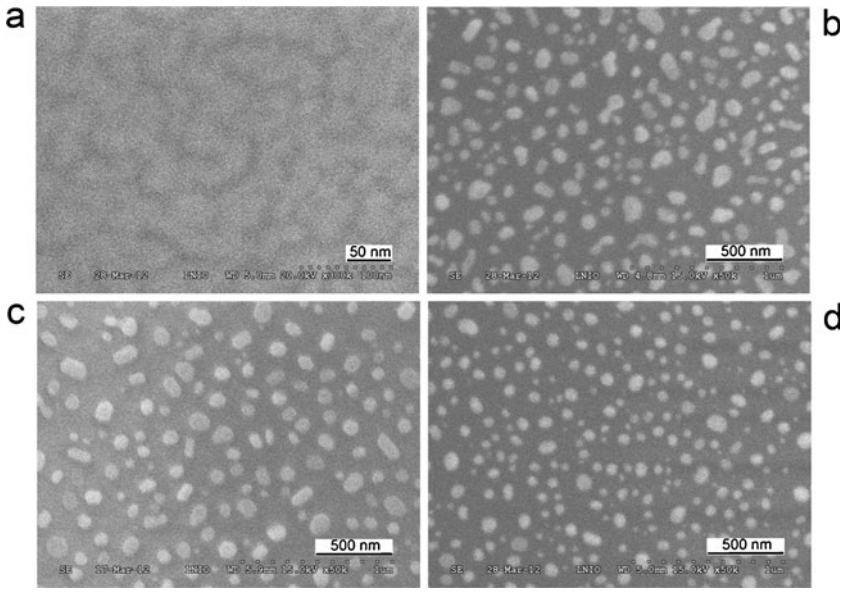

Fig. 5 The SEM images for glass samples modified with gold of 5 nm nominative thickness before (a) and after (b, c, d) annealing at 500 °C, 550 °C and 600 °C for 8 hrs. The scale bar is 50 nm for (a) and 500 nm for (b, c, d)

with a concomitant larger blue shift (27 nm) was observed when the annealing temperature was raised. It should be noted that a different plasmonic peak evolution was noticed for the annealed 8 nm sample when compared with those of 2 nm and 5 nm samples. Thus, higher annealing temperatures lead to large red-shift plasmonic resonances around 126 nm (from 654 nm at 500 °C to 780 nm at 600 °C annealing) with decreasing of OD value as 0.04. In addition, no matter what annealing temperature was used, the extinction LSPR-peak always became wider as the nominative thicknesses was increasing.

As mentioned, the thermal annealing of metal films promotes an interparticle separation in order to decrease the surface tension energy between NPs and substrate [50], which in turn enhances the affinity between gold nanoparticles and glass substrate. Additionally, the gold NPs obtained at higher annealing temperatures will become more homogeneous than those obtained at lower annealing temperature, where rounder NPs have sharper LSPR-spectra than inhomogeneous ones [51]. Such NPs characteristics are in agreement with our results for the 2 nm and 5 nm gold thicknesses. As clearly shown in Fig. 5, the freshly gold-evaporated sample (Fig.5a) with 5 nm nominative thicknesses has the feature morphology of continuous film containing many tiny grooves, which are consistent with its typical continuous film LSPR spectra in Fig. 2. All the

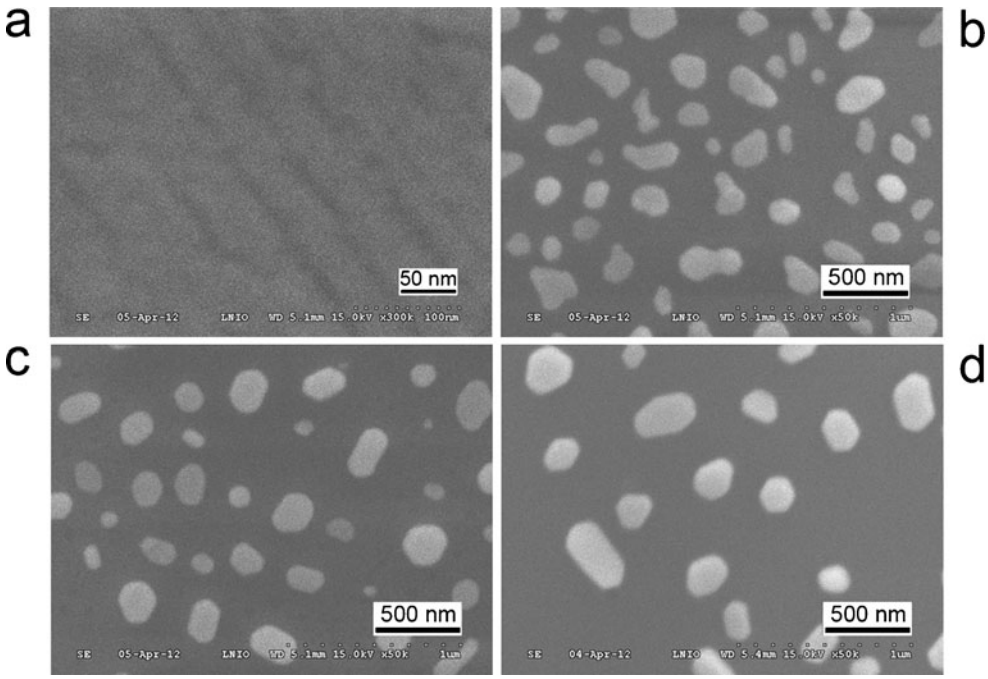

Fig. 6 The SEM images for glass samples modified with gold of 8 nm nominative thickness before (a) and after (b, c, d) annealing at 500 °C, 550 °C and 600 °C for 8 hrs. The scale bar is 50 nm for (a) and 500 nm for (b, c, d)

annealed samples have developed large area of well distributed gold nano-particles with a logical size evolution once the annealing temperature was increased. Round GNPs were predominantly formed at 600 °C when compared with those obtained at 500 °C and 550 °C, where the particles of various shapes were obtained (Fig. 5 b, c and d for the three annealing temperatures). These results can be interpreted by a better homogeneity of GNPs shapes after higher temperature annealing.

Since the LSPR spectra of 8 nm thickness sample have totally different characteristics at a given annealing temperature, when compared with those of 2 nm and 5 nm thicknesses sample (Fig. 4), the SEM topography characterization was employed and the results were shown in Fig. 6. For 8 nm "almost" continue evaporated gold film, similar groove-like structures as in case of 5 nm thicknesses were observed (Fig.6a). These results are corroborated with the previous results shown in Fig 2. However, for the annealed surface, the size of nanoparticles was evidently increased after annealing at higher temperature, which would be the reason for the red-shift of resonant wavelength at higher annealing temperature.

In conclusion, the annealing temperature has complex influence through the plasmonic extinction peak evolution when compared with the use of various gold film thicknesses. Since the increasing of annealing temperature induced different plasmonic peak evolutions (wavelength shift, intensity or shape changes), the authors assume that there would be a critical film thickness, where maybe several mechanisms are responsible for distinct annealing temperature dependent plasmonic properties.

There are few reports pointing out the existence of stability of gold nano-structures on glass substrate in the beginning of thermal annealing around 15 min. Therefore, the authors suppose that thermal exposure for longer periods of times may contribute to the sinking of gold nanoparticles partially inside glass [48]. Based on these assumptions, thermal pre-incubation studies before achieving the desired high annealing temperature have been conducted. Experimentally, it was studied the LSPR

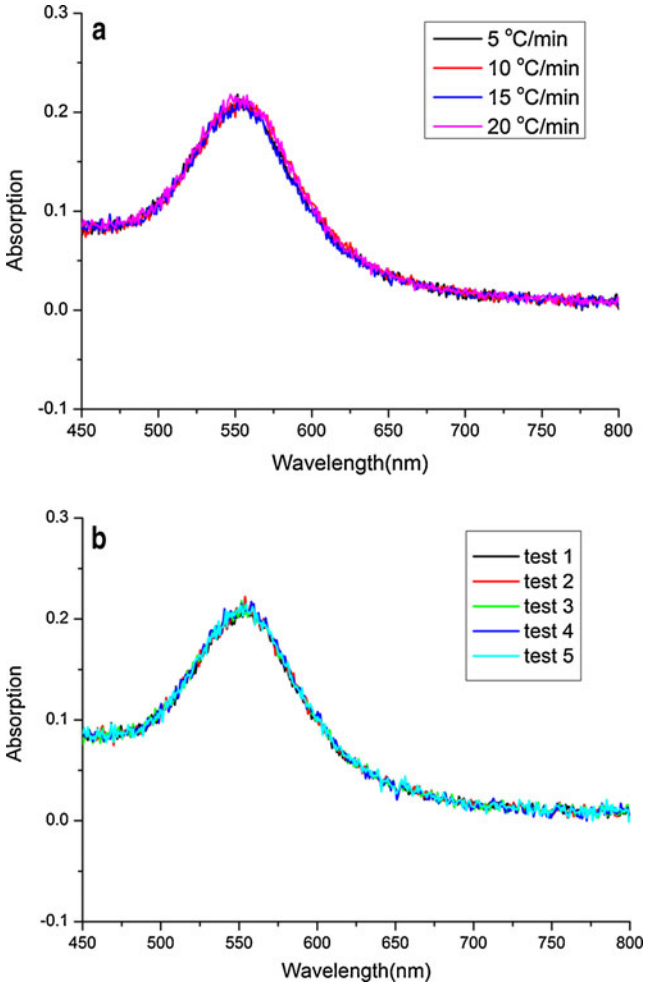

Fig. 7 The LSPR spectra for annealed sample with different initial thermal history (a) and stable optical response of homogenous surface (b), test 1 to test 5 means the different points measured around 1 cm^2 area on nano-structured surface

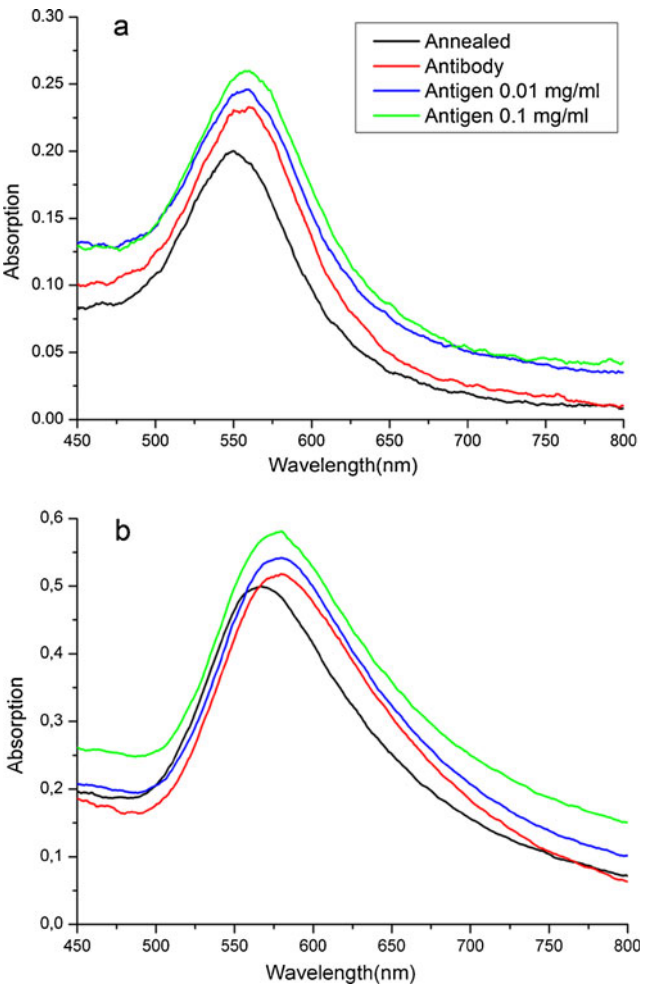

Fig. 8 The LSPR spectra of two different gold nano-structured surfaces with evaporated film of 2 nm (a) and 5 nm (b) subjected to different biofunctionalization steps for atrazine detection

properties of 2 nm sample subject to different temperature increases rate from room temperature up to 550 °C. As shown in Fig.7a, after annealing at 550 °C for 8 hrs, the plasmon peak amplitude and resonant wavelength are independent of thermal history prior to high temperature annealing. Thus, the LSPR spectra were only dependent of film thickness and annealing temperature. Additionally, very reproducible LSPR spectra were recorded in a relative large test area (about 1 cm^2) (Fig.7b). Based on these results, the protocol of evaporation followed by annealing near glass transition temperature of substrate was considered as an effective methodology to obtain stable LSPR nano-structures with excellent plasmonic tunability, which could be very advantageous in term of large scale fabrication of LSPR surface.

Plasmonic Biodetection of Atrazine

The biosensing ability of the gold annealed nano-structures was evaluated by the LSPR technique by using monoclonal anti-atrazine antibody and its specific antigen (atrazine) recognition sites. It was found that the functionalization increased the surrounding effective refractive index with visible modifications of plasmonic spectra, as shown in Fig.8a. Moreover, for the sample of 2 nm gold thicknesses, the resulted annealed surface showed a well-defined plasmon peak at 549 nm with OD value of 0.18 after stabilization with ethanol. Further, the immobilization of antibodies molecules was performed and leaded to red shift of 6 nm of extinction peak at 555 nm concomitant with an increase of OD to 0.22. Next, the specific binding of atrazine antigen to its antibodies contributes to increases of OD value from 0.23 to 0.26 for 0.01 mg/mL and 0.1 mg/mL atrazine, respectively, while the resonant wavelength for the antigen bonded surface remains unchanged at 556 nm. For the sample of 5 nm thickness (Fig.8b), the immobilization of same content of antibody onto the annealed gold surface leads to a larger wavelength red shift of 15 nm, which is in good agreement with the higher OD obtained for the 5 nm thick film (see Fig. 3.a) and that can be explained by a better surface coverage. Finally, the binding of antigen dilutions also leads to the increase of the OD value without obvious wavelength shift.

Conclusion

Crystalline gold nano-structures were prepared by electron beam evaporation approach followed by the high annealing temperature procedure. The influence of different gold evaporated thicknesses (2 nm, 5 nm and 8 nm) and annealing temperatures (500 °C, 550 °C and 600 °C) through the LSPR spectra were investigated. For samples with smaller nominative thicknesses (2 nm and 5 nm), the isotropic effects due to higher temperature annealing was responsible for blue-shifted and sharper plasmonic peaks, while for the sample with larger film thicknesses (8 nm), the size increasing effect contributed to the plasmonic peak evolution. In term of atrazine biodetection, the sample with thicker film (5 nm) exhibited better sensitivity, thanks to the well defined gold nanoparticles density.

Acknowledgments The authors are grateful for the financial support of the Stratégique Program 2009–2012 from University of Technology of Troyes (UTT) and to the France-Israel bilateral Research Network Programme 2009–2011. The ANR program ANR-07-Nano-032 "NP/CL" is also acknowledged for supplement of the optical set-up. The authors thank François Weil (LASMIS-UTT team) for providing the thermal processing equipment, Wang Huan and Rafael Salas-Montiel (UTT) for the fruitful discussions about the plasmonic evolution of metal nano-structures and for their experimental assistance.

Kun Jia thanks the Chinese Scholarship Council for funding his PhD scholarship in France.

References

1. Daniel MC, Astruc D (2004) Gold nanoparticles: assembly, super molecular chemistry, quantum-size-related properties, and applications toward biology, catalysis, and nanotechnology. Chem Rev 104:293–346
2. Wittstock A, Zielasek V, Biener J, Friend CM, Baumer M (2010) Nanoporous gold catalysts for selective gas-phase oxidative coupling of methanol at low temperature. Science 327:319–322
3. Schwerdtfeger P (2003) Gold goes nano—from small clusters to low-dimensional assemblies. Angew Chem Int Ed 42:1892–1895
4. Grzelczak M, Perez-Juste J, Mulvaney P, Liz-Marzan LM (2008) Shape control in gold nanoparticle synthesis. Chem Soc Rev 37:1783–1791
5. KimLing J, Maier M, Okenve B, Kotaidis V, Ballot H, Plech A (2006) Turkevich method for gold nanoparticle synthesis revisited. J Phys Chem B 110:15700–15707
6. Hu JQ, Wang ZP, Li JH (2007) Gold nanoparticles with special shapes: controlled synthesis, surface-enhanced Raman scattering, and the application in biodetection. Sensors 7:3299–3311
7. Saha K, Agasti SS, Kim C, Li XN, Rotello VM (2012) Gold nanoparticles in chemical and biological sensing. Chem Rev 112:2739–2779
8. Grand J, Adam PM, Grimault AS, Vial A, Lamy de la Chapelle M, Bijeon JL, Kostcheev S, Royer P (2006) Optical extinction spectroscopy of oblate, prolate and ellipsoid shaped gold nanoparticles: experiments and theory. Plasmonics 1:135–140
9. Grand J, Lamy de la Chapelle M, Bijeon JL, Adam PM, Vial A, Royer P (2005) Role of localized surface plasmons in surface-enhanced Raman scattering of shape-controlled metallic particles in regular arrays. Phys Rev B 72:033407
10. Sobhan MA, Withford MJ, Goldys EM (2010) Enhanced stability of gold colloids produced by femtosecond laser synthesis in aqueous solution of CTAB. Langmuir 26:3156–3159
11. Reed JA, Cook A, Halaas DJ, Parazzoli P, Robinson A, Matula TJ, Grieser F (2003) The effects of microgravity on nanoparticles size distributions generated by the ultrasonic reduction of an aqueous gold-chloride solution. Ultrason Sonochem 10:285–289
12. Turkevich J, Stevenson PC, Hillier J (1951) A study of the nucleation and growth processes in the synthesis of colloidal gold. Discuss Faraday Soc 11:55–75
13. Brust M, Walker M, Bethell D, Schiffrin DJ, Whyman R (1994) Synthesis of thiol-derivatised gold nanoparticles in a two-phase liquid-liquid system. J Chem Soc Chem Commun 7:801–802

14. Philip D (2009) Honey mediated green synthesis of gold nanoparticles. Spectrochim Acta A 73:650–653
15. Kumar V, Yadav SK (2009) Plant-mediated synthesis of silver and gold nanoparticles and their applications. J Chem Technol Biot 84:151–157
16. Xie JP, Zheng YG, Ying JY (2009) Protein-directed synthesis of highly fluorescent gold nanoclusters. J Am Chem Soc 131:888–889
17. Chen CF, Tzeng SD, Chen HY, Lin KJ, Gwo S (2008) Tunable plasmonic response from alkanethiolate-stabilized gold nanoparticle superlattices: evidence of near-field coupling. J Am Chem Soc 130:824–826
18. Zhao LL, Kelly KL, Schatz GC (2003) The extinction spectra of silver nanoparticle arrays: influence of array structure on plasmon resonance wavelength and width. J Phys Chem B 107:7343–7350
19. Chan GH, Zhao J, Schatz GC, Van Duyne RP (2008) Localized surface plasmon resonance spectroscopy of triangular aluminum nanoparticles. J Phys Chem C 112:13958–13963
20. Hutter E, Fendler JH (2004) Exploitation of localized surface plasmon resonance. Adv Mater 16:1685–1706
21. Willets KA, Van Duyne RP (2007) Localized surface plasmon resonance spectroscopy and sensing. Annu Rev Phys Chem 58:267–297
22. Hao F, Sonnefraud Y, Dorpe PV, Maier SA, Halas NJ, Nordlander P (2008) Symmetry breaking in plasmonic nanocavities: subradiant LSPR sensing and a tunable Fano resonance. Nano Lett 8:3983–3988
23. Viste P, Plain J, Jaffiol R, Vial A, Adam PM, Royer P (2010) Enhancement and quenching regimes in metal–semiconductor hybrid optical nanosources. ACS Nano 4:759–764
24. Barbillon G, Bijeon JL, Bouillard JS, Plain J, Lamy de la Chapelle M, Adam PM, Royer P (2008) Detection in the near-field domain of biomolecules adsorbed on a single metallic nanoparticle. J Microsc 229:270–274
25. EI-Sayed IH, Huang XH, EI-Sayed MA (2005) Surface plasmon resonance scattering and absorption of anti-EGFR antibody conjugated gold nanoparticles in cancer diagnostics: applications in oral cancer. Nano Lett 5:829–834
26. Tong L, Cobley CM, Chen JY, Xia YN, Cheng JX (2010) Bright three-photon luminescence from gold/silver alloyed nanostructures for bioimaging with negligible photothermal toxicity. Angew Chem Int Ed 49:3485–3488
27. Huang XH, Jain PK, EI-Sayed IH, EI-Sayed MA (2008) Plasmonic photothermal therapy (PPTT) using gold nanoparticles. Lasers Med Sci 23:217–228
28. McMahon JM, Henry AI, Wustholz KL, Natan MJ, Freeman RG, Van Duyne RP, Schatz GC (2009) Gold nanoparticle dimer plasmonics: finite element method calculations of the electromagnetic enhancement to surface-enhanced Raman spectroscopy. Anal Bioanal Chem 394:1819–1825
29. Xia YN, Halas NJ (2005) Shape-controlled synthesis and surface plasmonic properties of metallic nanostructures. MRS Bull 30:338–348
30. Sagle LB, Ruvuna LK, Ruemmele JA, Van Duyne RP (2011) Advances in localized surface plasmon resonance spectroscopy biosensing. Nanomedicine 6:1447–1462
31. Homola J, Yee SS, Gauglitz G (1999) Surface plasmon resonance sensors: review. Sens Actuat B-Chem 54:3–15
32. Bellapadrona G, Tesler AB, Grunstein D, Hossain LH, Kikkeri R, Seeberger PH, Vaskevich A, Rubinstein I (2012) Optimization of localized surface plasmon resonance transducers for studying carbohydrate-protein interactions. Anal Chem 84:232–240
33. Kalyuzhny G, Vaskevich A, Schneeweiss MA, Rubinstein I (2002) Transmission surface-plasmon resonance (T-SPR) measurements for monitoring adsorption on ultrathin gold island films. Chem Eur J 8:3849–3857
34. Lee SW, Lee KS, Ahn JY, Lee JJ, Kim MG, Shin YB (2011) Highly sensitive biosensing using arrays of plasmonic Au nanodisks realized by nanoimprint lithography. ACS Nano 5:897–904
35. Murphy CJ, Gole AM, Hunyadi SE, Stone JW, Sisco PN, Alkilany A, Kinard BE, Hankins P (2008) Chemical sensing and imaging with metallic nanorods. Chem Commun 544–557
36. Rindzevicius T, Alaverdyan Y, Dahlin A, Hook F, Sutherland DS, Kall M (2005) Plasmonic sensing characteristics of single nanometric holes. Nano Lett 5:2335–2339
37. Hu M, Chen JY, Li ZY, Au L, Hartland GV, Li XD, Marquez M, Xia YN (2006) Gold nanostructures: engineering their plasmonic properties for biomedical applications. Chem Soc Rev 35:1084–1094
38. Doron-Mor I, Barkay Z, Filip-Granit N, Vaskevich A, Rubinstein I (2004) Ultrathin gold island films on silanized glass. morphology and optical properties. Chem Mater 16:3476–3483
39. Piscopiello E, Tapfer L, Antisari MV, Paiano P, Prete P, Lovergine N (2008) Formation of epitaxial gold nanoislands on (100) silicon. Phys Rev B 78:035305
40. Szunerits S, Praig VG, Manesse M, Boukherroub R (2008) Gold island films on indium tin oxide for localized surface plasmon sensing. Nanotechnology 19:195712
41. Gluodenis M, Manley C, Foss CA (1999) In situ monitoring of the change in extinction of stabilized nanoscopic gold particles in contact with aqueous phenol solutions. Anal Chem 71:4554–4558
42. Grabar KC, Freeman RG, Hommer MB, Natan MJ (1995) Preparation and characterization of Au colloid monolayers. Anal Chem 67:735–743
43. Jian Y, Bonroy K, Nelis D, Frederix F, D'Haen J, Maes G, Borghs G (2008) Enhanced localized surface plasmon resonance sensing on three-dimensional gold nanoparticles assemblies. Colloids Surf A 321:313–317
44. Ruach-Nir I, Bendikov TA, Doron-Mor I, Barkay Z, Vaskevich A, Rubinstein I (2007) Silica-stabilized gold island films for transmission localized surface plasmon sensing. J Am Chem Soc 129:84–92
45. Karakouz T, Tesler AB, Bendikov TA, Vaskevich A, Rubinstein I (2008) Highly stable localized plasmon transducers obtained by thermal embedding of gold island films on glass. Adv Mater 20:3893–3899
46. Karakouz T, Holder D, Goomanovsky M, Vaskevich A, Rubinstein I (2009) Morphology and refractive index sensitivity of gold island film. Chem Mater 21:5875–5885
47. Karakouz T, Maoz BM, Lando G, Vaskevich A, Rubinstein I (2011) Stabilization of gold nanoparticle films on glass by thermal embedding. ACS Appl Mater Interfaces 3:978–987
48. Tesler AB, Chuntonov L, Karakouz T, Bendikov T, Haran G, Vaskevich A, Rubinstein I (2011) Tunable localized plasmon transducers prepared by thermal dewetting of percolated evaporated gold films. J Phys Chem C 115:24642–24652
49. Gao SY, Koshizaki N, Tokuhisa H, Koyama E, Sasaki T, Kim JK, Ryu J, Kim DS, Shimizu Y (2010) Highly stable Au nanoparticles with tunable spacing and their potential application in surface plasmon resonance biosensors. Adv Func Mater 20:78–86
50. Yan CJ, Chen YC, Jin A, Wang M, Kong XD, Zhang XF, Ju Y, Han L (2011) Molecule oxygen-driven shaping of gold islands under thermal annealing. Appl Surf Sci 258:377–381
51. Zhang XM, Zhang JH, Wang H, Hao YD, Zhang X, Wang TQ, Wang YN, Zhao R, Zhang H, Yang B (2010) Thermal-induced surface plasmon band shift of gold nanoparticle monolayer: morphology and refractive index sensitivity. Nanotechnology 21:465702